OPEN ACCESS
IOP Publishing

Letters
Reports on Progress in Physics

Rep. Prog. Phys. **88** (2025) 070501 (8pp)
https://doi.org/10.1088/1361-6633/adeebb

Letter

Strong field physics in open quantum systems

Neda Boroumand[1], Adam Thorpe[1], Graeme Bart[1], Andrew M Parks[2], Mohamad Toutounji[3], Giulio Vampa[4], Thomas Brabec[1,*] and Lu Wang (汪璐)[1,*]

[1] Department of Physics, University of Ottawa, Ottawa, Ontario K1N 6N5, Canada
[2] Wyant College of Optical Sciences, University of Arizona, Tucson, AZ, United States of America
[3] College of Science, Department of Chemistry, UAE University, Al-Ain, United Arab Emirates
[4] Joint Attosecond Science Laboratory, National Research Council of Canada and University of Ottawa, 100 Sussex Drive, Ottawa, Ontario K1A 0R6, Canada

E-mail: Thomas.brabec@uottawa.ca and lu.wangTHz@outlook.com

Received 21 March 2025, revised 29 June 2025
Accepted for publication 11 July 2025
Published 18 July 2025

Corresponding editor: Dr Paul Mabey

Abstract

Dephasing is the loss of phase coherence due to the interaction of an electron with the environment. The most common approach to model dephasing in light–matter interaction is the relaxation time approximation. Surprisingly, its use in intense laser physics results in a pronounced failure, because ionization is highly overestimated. Here, this shortcoming is corrected by developing a strong field model in which the many-body environment is represented by a heat bath. Our model reveals that ionization enhancement and suppression by several orders of magnitude are still possible, however only in more extreme parameter regimes. Our approach allows the integration of many-body physics into intense laser dynamics with minimal computational and mathematical complexity, thus facilitating the identification of novel effects in strong-field physics and attosecond science.

Supplementary material for this article is available online

Keywords: strong field physics, relaxation time approximation, quantum optics, open quantum system

* Authors to whom any correspondence should be addressed.

1. Introduction

Strong laser-matter interaction is commonly modeled as a closed quantum system with a single active electron [1, 2]. While this assumption is well justified for atomic gases, its validity is not so clear for denser materials, such as liquids and solids. A full many-body treatment of the non-perturbative dynamics of all electrons and nuclei is prohibitively difficult. Therefore, it is more practical to model dense materials as a single active electron within an open quantum system, where many-body effects are accounted for by interactions with the environment [3–5]. Due to its simplicity, the environment in intense laser-driven solids is mostly modeled in the relaxation time approximation [6, 7], where the effect of many-body dynamics is replaced by a dephasing time T_2 [8–10]. Here, the relaxation time approximation only refers to the dephasing term T_2, not the energy relaxation time T_1. In particular, the T_2 represents a constant decay of the dynamics of off-diagonal density matrix elements ($\rho_{ij}, i \neq j$) i.e. loss of coherence. Note that dephasing is also commonly referred to by Γ [11]. In our case $\Gamma = 1/T_2$. For dielectrics, the T_2 is typically around a few femtoseconds [6, 12, 13].

However, a simple calculation for an under-resonantly driven two-level system reveals questionable features of the relaxation time approximation in accurately predicting ionization [14]. Following the conventional optical ionization theory, we refer to ionization as the laser-induced excitation of an electron from the valence $|0\rangle$ to the conduction $|1\rangle$ band. In figure 1(a) the ionization dynamics with dephasing described via the relaxation time approximation (yellow $\sim 10^{-1}\%$) and without dephasing (blue $\sim 10^{-8}\%$) are compared. It can be seen that the relaxation time approximation predicts $10^{-1}\%$ ionization under a very moderate electric field strength $E_0 = 5 \times 10^8\,\mathrm{V\,m^{-1}}$.

This is clearly unphysical because laser damage of semiconductors (ZnO, for example) occurs around $5 \times 10^9\,\mathrm{V\,m^{-1}}$. This leads to laser induced free carrier density $\sim 10^{22}\,\mathrm{cm^{-3}}$ [15, 16], equivalent to $\sim 5\%$ ionization based on the atomic density $\sim 2 \times 10^{23}\,\mathrm{cm^{-3}}$ [17]. For weak electric field $5 \times 10^8\,\mathrm{V\,m^{-1}}$, the expected free carrier density is $\sim 10^{16}\,\mathrm{cm^{-3}}$ corresponding to ionization $\sim 10^{-6}\%$ [18]. By comparing $\sim 10^{-6}\%$ to the yellow curve in figure 1(a) ($\sim 10^{-1}\%$), we can see that the relaxation time approximation overestimates the ionization by five orders of magnitude.

Many attempts have been made to mitigate the overestimation of ionization [12, 13, 19–21]. However, the underlying issue is still not resolved. Dephasing typically refers to the loss of coherence between two energy levels and is generally considered separate from excitation or transition processes. However, our results indicate that when the phase relationship between the laser field and the two-level system is disrupted, virtually excited electrons are prevented from returning to the ground state. This leads to a real transition i.e. a change in population distribution in the two-level system after the laser pulse is gone. We refer to the resulting ionization enhancement as *dephasing ionization*. The apparent shortcomings of the relaxation time approximation leave a gap between more complex and computationally demanding many-body approaches and oversimplified dephasing models commonly used in intense light–matter interaction.

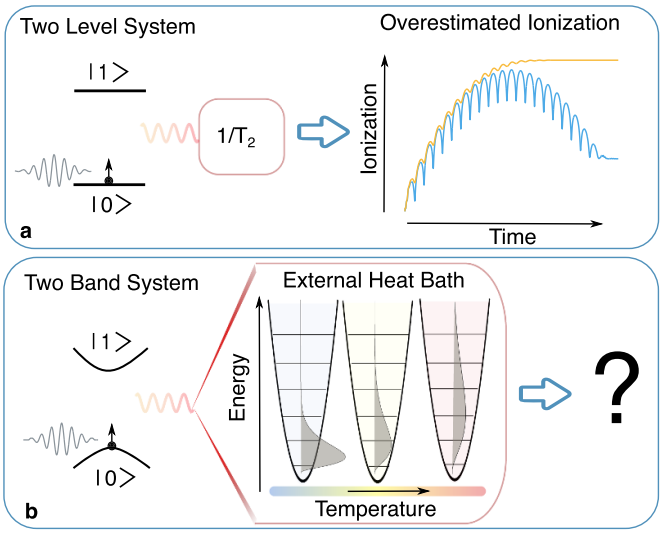

Figure 1. Illustration of under-resonantly driven, open two-level/band systems. Panel (a) presents the two-level system (band gap $E_g = 3.51$ eV) described by the relaxation time approximation. On the right-hand side, ionization with ($T_2 = 6$ fs, yellow curve) and without dephasing ($T_2 = \infty$, blue curve) is compared. A moderate electric field strength $E_0 = 5 \times 10^8\,\mathrm{V\,m^{-1}}$ with photon energy ~ 0.39 eV ($\lambda_0 = 3.2\,\mu$m) is chosen (see supplement figure S5 for details). Panel (b) shows the two-band system coupled to a heat bath described via the spin-boson model. The heat bath is modeled using boson harmonic oscillator modes. As the temperature rises, boson modes with higher energies are engaged (gray curves).

Furthermore, ionization is the first step in all strong field processes, such as material machining [22–24], petahertz electronics [25, 26], electron acceleration from nano emitters [27], and high-harmonic generations [2, 28]. Due to the importance of ionization, a deeper understanding of dephasing ionization is essential.

As such, a more sophisticated model is needed that ideally maintains most of the simplicity and wide applicability of the relaxation time approximation. We borrow inspiration from the field of open quantum systems and adopt one of its key achievements, the spin-boson model, which typically serves as a minimal model to describe the quantum dynamics of an electron under the influence of the environment [29–31]. Here, the spin-boson model is integrated into the semiconductor Bloch equations governing intense laser solid-state physics. The electron dynamics is represented by a single electron–hole, two-band model which is linearly coupled to its environment via bosonic harmonic oscillator modes, see figure 1(b). The so-called strong field spin-boson (SFSB) model allows for a closed-form solution of the electron dynamics in an environment and in the presence of an intense laser. We refer to the environment as a heat bath in the rest of the paper.

The SFSB model fixes the pathological ionization behavior displayed by the relaxation time approximation. Nevertheless, numerical analysis of the SFSB equation reveals that ionization enhancement of up to a few orders

of magnitude is still possible, but only at high temperatures. Interestingly, in the opposite low-temperature limit the heat bath can suppress ionization by up to a few orders of magnitude, which we term as *dephasing suppressed ionization*. This occurs when the electron and heat bath interact strongly.

The SFSB model provides a distinctive approach to uncovering the physics of complex many-body systems with minimal computational and mathematical complexity. The predictive power of the SFSB approach can be progressively refined through either more detailed models or by fine-tuning the heat bath response through comparison with experiments. We anticipate that the SFSB framework will facilitate the discovery of new phenomena in strong-field physics and attosecond science.

2. Theory

Our analysis starts with a single electron two-band system coupled to a bosonic heat bath via a linear interaction term, [32, 33]

$$H = -\frac{1}{2}\mathcal{E}\left(\boldsymbol{K}_t,t\right)\sigma_z + \frac{1}{2}\hbar\Omega\left(\boldsymbol{K}_t,t\right)\sigma_x + \sum_q \hbar\omega_q b_q^\dagger b_q + \sigma_z \sum_q g_q\left(b_q + b_q^\dagger\right). \quad (1)$$

Here, $\mathbf{E}(t)$ is the laser electric field, the vector potential is defined by $-\partial_t\mathbf{A} = \mathbf{E}$, and $\boldsymbol{K}_t = \boldsymbol{K} + e\boldsymbol{A}(t)/\hbar$. The canonical momentum $\boldsymbol{K}$ belongs to the shifted Brillouin zone $\overline{\mathrm{BZ}}$. Further, $\Omega(\boldsymbol{K}_t,t) = (2e/\hbar)\mathbf{d}(\boldsymbol{K}_t,t)\mathbf{E}(t)$ is a generalized Rabi frequency, $e > 0$ is the elementary charge and $\hbar$ is the reduced Planck constant; $\mathbf{d}(\boldsymbol{K}_t,t)$ and $\mathcal{E}(\boldsymbol{K}_t,t)$ represent transition dipole and bandgap between conduction $|1\rangle$ and valence $|0\rangle$ band, respectively. The time dependence of these quantities arises from the moving momentum frame. The Pauli matrices are denoted by σ_j $(j = x,y,z)$. Finally, ω_q, $\hat{b}_q^\dagger$, $\hat{b}_q$, and g_q are the harmonic oscillator frequency, creation, and annihilation operators, and the coupling coefficient of a mode with momentum $\mathbf{q}$, respectively. In particular, the work [34] suggests that the coupling strength g_q is proportional probability distributions of the bosonic environment of mode q. This coupling term proportional to g_q in equation (1) is a generic form and is valid for strong field interactions of electron-plasmon [35], electron-phonon [36], and electron-exciton. Besides, g_q can be directly calculated via the ab-initio method, which corresponds to the scattering matrix element between the initial and the final state [34–36]. Here we refer to the interactions between the electron (in the two-band system) and the exciton or plasma as collective electron interactions.

The coupling term between the heat bath and the two-band system appears exclusively in the diagonal terms of the Hamiltonian. Thus, it accounts only for dephasing, and not directly for heat-bath driven transitions between bands, i.e the off-diagonal terms. Nevertheless, due to the coupling of laser and heat bath driven dynamics [6, 37], dephasing does influence the overall ionization. In the high-temperature limit, multi-boson transitions between valence and conduction band could become relevant but are ignored here.

The Hamiltonian shown in equation (1) can be further simplified. First, we perform a polaron transformation that diagonalizes the laser-free Hamiltonian [38]. This is followed by a change to the interaction picture, which results in

$$H_I = -\frac{\mathcal{E}\left(\boldsymbol{K}_t,t\right)}{2}\sigma_z + \frac{1}{2}\hbar\Omega\left(\boldsymbol{K}_t,t\right)\left(\sigma_+ D^{\dagger^2} + \sigma_- D^2\right). \quad (2)$$

For a detailed derivation, see supplementary material, section I. Here, $\sigma_+ = (\sigma_x + i\sigma_y)/2$ and $\sigma_- = (\sigma_x - i\sigma_y)/2$. The interactions with laser and heat bath are now described by a single term, with the shift operator defined as $D(t) = \exp\left\{-\sum_q g_q\left[b_q^\dagger(t) - b_q(t)\right]/(h\omega_q)\right\}$.

The evolution of the density matrix is determined by the integration of the Liouville–Von Neumann equation with the Hamiltonian shown in equation (2). Initially, the valence band is fully occupied, the conduction band is empty, and the heat bath is in thermal equilibrium. A closed-form solution is obtained by using a Dyson expansion up to the second order. As we are only interested in the two-band system dynamics, the heat bath degrees of freedom are traced out (see supplementary material sections II and III for details) [9, 32, 33, 39–46]. We found that the dominant contribution to ionization is contained in the second order expansion term [44] from which the conduction band population follows as

$$n_c\left(\boldsymbol{K},t\right) = \frac{1}{2}\mathrm{Re}\left\{\int_{-\infty}^{t}\int_{-\infty}^{t_1}\Omega^*\left(\boldsymbol{K}_{t_1},t_1\right)\Omega\left(\boldsymbol{K}_{t_2},t_2\right) \times \exp\left[iS\left(t_1,t_2\right) + C\left(t_1 - t_2\right)\right]dt_1 dt_2\right\}, \quad (3)$$

$$n_c\left(t\right) = \int_{\overline{\mathrm{BZ}}} n_c\left(\boldsymbol{K},t\right)d\boldsymbol{K}, \quad (4)$$

where the action $S(t_1,t_2) = \int_{t_2}^{t_1} d\tau\,\mathcal{E}_s(\boldsymbol{K}_\tau,\tau)/\hbar$, and $\mathcal{E}_s(\boldsymbol{K}_\tau,\tau) = \sqrt{\mathcal{E}(\boldsymbol{K}_\tau,\tau)^2 + |\hbar\Omega(\boldsymbol{K}_\tau,\tau)|^2}$ is the bandgap shifted by the dynamic Stark effect [44, 47, 48]. As equation (3) suggests, all the environment (heat bath) influences are exclusively included by the correlation function $C(t_1 - t_2)$. Typically, the correlation function indicates that the future evolution of the system depends not only on its instantaneous state but also on its past history [4, 49]. Specifically, the correlation function is defined as:

$$C\left(t_1 - t_2\right) \approx \int_{-\infty}^{\infty} J\left(\omega\right)\left\{i\sin\left[\omega\left(t_1 - t_2\right)\right] - \left\{1 - \cos\left[\omega\left(t_1 - t_2\right)\right]\right\}\coth\left(\frac{\hbar\omega}{2k_B T}\right)\right\}d\omega, \quad (5)$$

where k_B is the Boltzmann constant. The temperature T dependence in equation (5) is contained only in the coth term. The g_q coefficient in equations (1) and (2) are replaced by a spectral density $J(\omega)$ through a transition from discrete to continuous modes. The spectral density depends on two parameters: coupling strength j_o, and cutoff frequency ω_c. There exists a wealth of different models for the spectral density $J(\omega)$, such as the Debye [43], Ohmic [9], Under-Damped

Brownian [33, 45], Gaussian [46], and Shifted-Gaussian models, the definition of which can be found in the supplementary material, section IV.

The relaxation time approximation is recovered for the Debye bath in the high T-limit, $C(t_1 - t_2) \to -(t_1 - t_2)/T_2$ with $T_2 = \hbar/(2\pi k_B T j_o)$, as outlined in the supplementary material, section IV.A. By contrast, the high T-limits of the other heat bath models do not exhibit a linear time dependence in the exponent.

In the context of strong laser solid material interaction, the temperature T refers to the local electron or ion temperature. Our approach presents an approximation, as the system, its dependence on laser pulse duration, is not always in thermal equilibrium. This process is typically analyzed via the well-established two-temperature model [50–52], where the laser first heats the electrons, and the absorbed energy of the electrons is subsequently transferred to the lattice, increasing its temperature. Material damage or melting is typically determined by the lattice temperature. For dielectrics, damage occurs around a few thousand K, even though the electron temperature can be much higher, reaching up to 10^5 K [50–52]. While our approach can be extended to describe non-equilibrium heat baths, this would go beyond the limit of an initial investigation.

The cutoff frequency ω_c falls within the terahertz to the far-infrared range for phonons, and spans the far-infrared to the mid-infrared range for collective electronic excitations, such as excitons and plasmons. The coupling strength j_o is a dimensionless parameter ranging from 10^{-3} to multiples of unity [32, 33, 53–56]. For phonons, $j_o < 1$ in III–V semiconductors, whereas $j_o > 1$ in more polar II–VI compounds [3]. Strong electron-phonon coupling $j_o > 1$ typically occurs in very polar materials [55, 57] such as bi-layer graphene [58], single-layer InSe [59] and superconductors [60, 61]. For collective electronic excitations, the coupling strength depends on the electron density [35]. For electron densities above 10^{20} cm^{-3} and for $\hbar\omega_c \sim 1$ eV the plasmon coupling strength can become comparable to and even exceed the phonon coupling strength.

3. Results

We have selected zinc oxide (ZnO), a representative and widely studied semiconductor. The crystal momentum $\boldsymbol{k}$ dependence in the entire 3D Brillouin zone is considered for the two-band system. Material parameters are derived from *ab initio* calculations [62–64] (see supplementary material section V, table I). We find that both 3D and 1D calculations along the Γ-M direction yield similar results in terms of relative heat bath-induced ionization changes, both quantitatively and qualitatively (see supplementary material figure S4). Therefore, for computational efficiency, we focus on the 1D Brillouin zone along the Γ-M direction throughout the following calculations.

A driving laser with the center wavelength $\lambda_0 = 3.2\,\mu$m is selected. The center frequency is defined as $\omega_0 = 2\pi c/\lambda_0 \approx 2\pi \times 10^{14}$ Hz ($\hbar\omega_0 \sim 0.39$ eV) with c the vacuum light velocity. The energy of the laser photons is much lower than the resonance energy of ZnO (with a band gap of $\mathcal{E}_g = 3.51$ eV), meaning that at least 9 photons are required to excite an electron from the valence band to the conduction band. We choose a linearly polarized electric field defined as $\mathbf{E} = E_x = E_0 \exp\left(-t^2/\tau^2\right)\cos(\omega_0 t)$, where $\tau = 20$ fs. The electric field strength $E_0 = 1.5 \times 10^9$ V m^{-1} is well below the single pulse damage threshold of ZnO [65]. These parameter values are used throughout the paper unless otherwise stated.

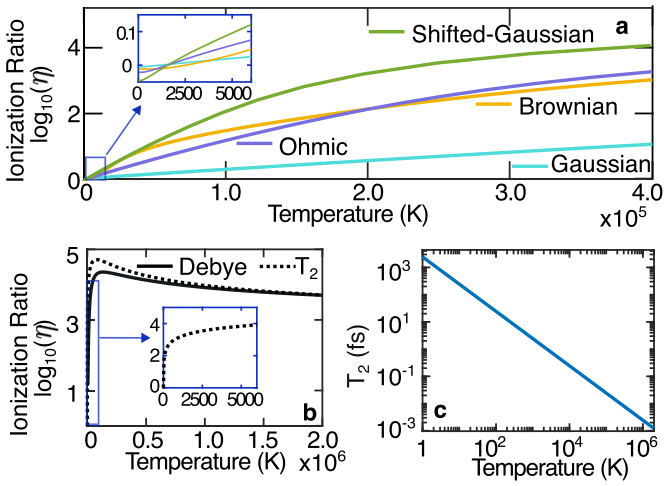

Figure 2. Panel (a) presents the ionization ratio versus temperature T for various heat baths. Panel (b) shows the ionization ratio for the Debye heat bath and relaxation time approximation versus T. The insets in (a) and (b) show details in the low T regime. The relaxation time $T_2 = \hbar/(2\pi k_B T j_o)$ obtained from the Debye spectral density, is plotted in (c) as a function of T. The heat bath parameters are $\omega_c = 0.1\omega_0$, $j_o = 0.1$.

The change of ionization due to the heat bath is characterized by calculating the ionization ratio with and without the heat bath,

$$\eta = \left.\frac{n_c\,(j_o \neq 0)}{n_c\,(j_o = 0)}\right|_{t=\infty}, \tag{6}$$

where $n_c(t)$ is defined in equation (4).

In figure 2(a), the ionization ratio $\log_{10}(\eta)$ is plotted versus T for Ohmic, Under-Damped Brownian, Gaussian, and Shift-Gaussian spectral densities, all of which follow a similar trend and yield comparable results. Thus, without loss of generality, we have chosen the Ohmic spectral density throughout the entire numerical analysis. The ionization ratio is plotted in $\log_{10}$ scale, where the positive (negative) numbers of $\log_{10}(\eta)$ correspond to the order of magnitude of enhancement (suppression) of ionization. Figure 2(b) shows that the Debye spectral density converges to the relaxation time approximation at very high temperatures. The temperature dependence of T_2, obtained from the Debye spectral density in the high T limit above, is presented in figure 2(c). Both Debye and relaxation time approximation show an unrealistic rise of η at low T and therefore do not represent realistic heat bath models. This is to be expected, due to the unphysically long high-frequency tail of the Debye spectral density [57, 66]. Finally, by comparing the zoomed-in sections of figures 2(a) and (b), one can see that the relaxation time approximation substantially overestimates

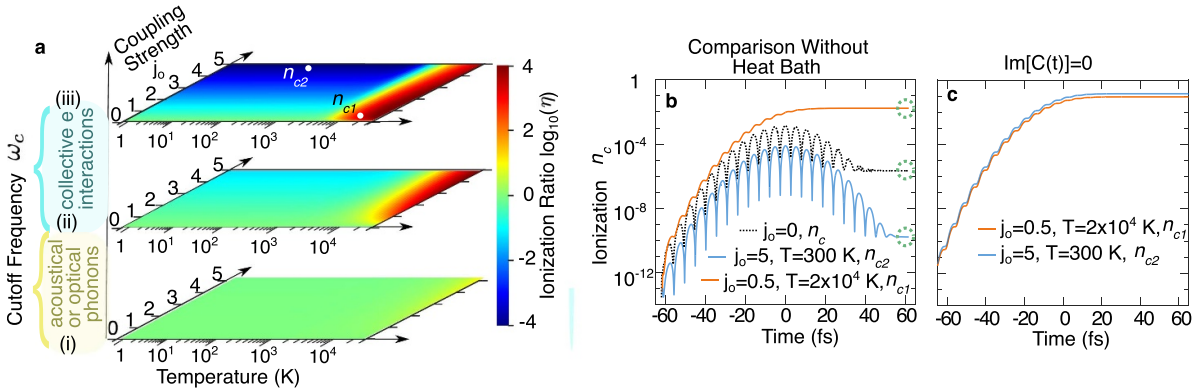

Figure 3. Panel (a) shows ionization ratio $\log_{10}(\eta)$ as a function of local temperature $T \in [1, 3\times10^4]$ K and coupling coefficient $j_o \in [0,5]$. The three panels represent different cutoff frequencies, (i) $\omega_c = 0.01\omega_0$, (ii) $\omega_c = 0.1\omega_0$ and (iii) $\omega_c = 2.1\omega_0$. (b) Ionization versus time for two data points n_{c1} and n_{c2} in panel (iii) of (a); the black dotted curve shows ionization in the absence of a heat bath. The three data points marked by circles at the end of the time coordinate are related to discussions in figure 4. (c) same as plots for n_{c1} and n_{c2} in (b) only with setting the imaginary part of the heat bath response $C(t)$ (defined in equation (5)) to zero.

ionization at low temperatures, while all the other heat baths in figure 2(a) show negligible changes in ionization, as detected by experiments.

In figure 3(a), the ionization ratio $\log_{10}(\eta)$ is scanned over a wide range of T and j_o. Although electrons are fermions, their collective excitations can, to a good approximation, be treated as bosons [33, 35, 57]. As such, they can be directly modeled via the spin-boson Hamiltonian shown in equation (1). These different quasi-particle excitations are mainly distinguished by the choice of the cutoff frequencies ω_c. As a result, in figure 3(a) we chose three representative values of cutoff frequencies: (i) $\omega_c = 0.01\omega_0$ represents optical and acoustic phonons which lie in the terahertz range (ii) $\omega_c = 0.1\omega_0$ represents collective electron excitations, and (iii) $\omega_c = 2.1\omega_0$ represents the plasma frequencies that extend into the UV range. From panel (i), we infer that phonon effects on ionization are minimal, except under extreme conditions such as high-temperature laser machining. In contrast, panel (iii) indicates that environmental influences on ionization become more significant at large cutoff frequencies, even with moderate coupling strength. Additionally, ionization enhancement occurs only at the high temperature limit, whereas ionization suppression is observed exclusively at the low temperature limit. These two limits are represented by data points n_{c1}, n_{c2} in panel (iii), for which, the temporal evolution of ionization is plotted in figure 3(b). The black dotted curve represents ionization in the absence of a heat bath $n_c(j_o = 0)$. While all T and ω_c ranges can be realized in intense laser-driven ZnO, the shown j_o-dependence is not ZnO specific. We explore the typical range of j_o defined above.

The increase and decrease of ionization can be explained by the real and imaginary parts of the correlation function $C(t)$. With a given ω_c, at extremely high temperatures, the correlation function approaches a delta function (instantaneous) in time, leading to the Markovian limit [67]. In this limit, the real part of the correlation function dominates, and one may neglect the imaginary contribution. This is why the relaxation time approximation using T_2 as a purely real number remains

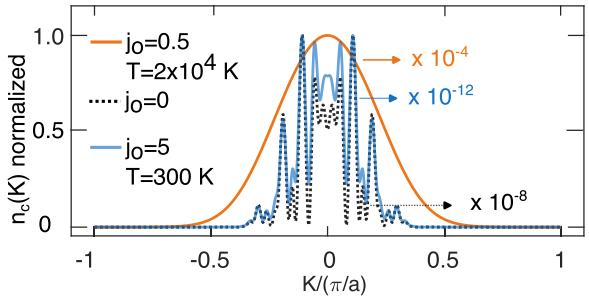

Figure 4. Ionization as a function of crystal momentum K. The ionization $n_c = \sum_i n_c(K_i)$ corresponds to the three data points marked by circles in figure 3(b).

a valid approximation at high temperatures. On the other hand, at low temperatures, the correlation function is non-Markovian with a wider distribution in time. In this case, the phase of the correlation function acts as a dynamic addition to the bandgap, increasing the original material bandgap, and thereby resulting in dephasing suppressed ionization. The importance of the heat bath phase becomes clear from a comparison of figures 3(b) and (c). In figure 3(c) the imaginary part of the $C(t)$ is set to zero, as a result of which ionization at $T = 300$ K changes from suppression into enhancement.

A possible experimental measurement of the n_c shown in figure 3 can be achieved via the angle-resolved photoemission spectroscopy (ARPES). Since ARPES typically presents the electron density as a function of the crystal momentum K, here in figure 4 we show n_c as a function of K after the driving field is gone. The curves are plotted using 800 evenly spaced mesh points. The ionization $n_c = \sum_i n_c(K_i)$ corresponds to three data points indicated by circles in figure 3(b). From figure 4, one can see that the dephasing ionization has a distinctive signature, markedly different from the optical ionization in the absence of an environment. On the other hand, dephasing suppressed ionization

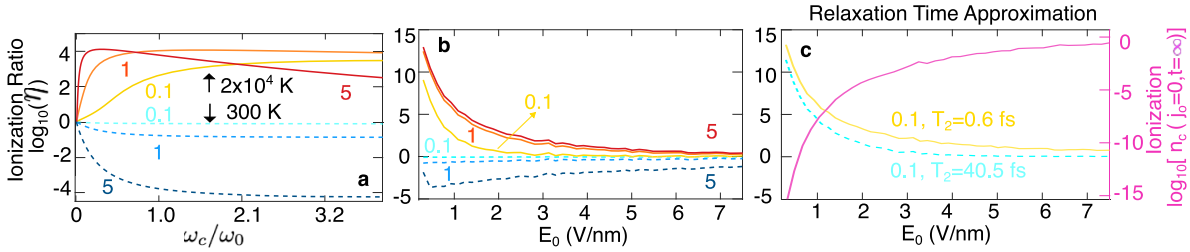

Figure 5. Ionization ratio as a function of cutoff frequency ω_c (panel (a)) and of peak electric field strength E_0 (panels (b) and (c)) are presented. We have chosen different values of $j_o \in \{0.1, 1, 5\}$ denoted by different colors beside each curve. The cold-colored dashed curves are for $T = 300$ K; warm-colored full curves refer to $T = 2 \times 10^4$ K. In (a), the ionization without the heat bath is $n_c(j_o = 0, t = \infty) = 2 \times 10^{-6}$. Panels (b) and (c) are calculated by $\omega_c = 0.4\omega_0$. The relaxation time used in panel (c) is calculated by $T_2 = \hbar/2\pi k_B j_o T$. The pink curve plotted on the right y axis shows the ionization $n_c(j_o = 0, t = \infty)$ in the absence of the heat bath.

behaves similarly to ionization without environmental influence.

This opens up the possibility of diagnostic measurements. For example, in a potential future experiment, the target material (ZnO) can be put in a cavity to modify the coupling to the environment. On the other hand, the ARPES results combined with our model can be used to retrieve the coupling coefficient j_o to the environment, which is otherwise nearly impossible to measure.

To further explore the parameter dependence, ionization ratios are plotted as functions of the cutoff frequency ω_c in figure 5(a) and as functions of the peak electric field strength E_0 in figures 5(b) and (c). Figure 5(c) presents the results calculated by relaxation time approximation. Two temperatures are considered: 300 K, shown by dashed curves in cool colors, and 2×10^4 K, shown by solid curves in warm colors. Each curve is color-coded according to the coupling strength j_o, with the corresponding j_o values labeled in matching colors.

Figure 5(a) confirms that dephasing ionization only occurs at high temperatures, while dephasing suppression ionization happens exclusively at low temperatures. Figure 5(b) indicates that the heat bath only plays a role at moderate electric field strengths. This can be explained by the multi-photon and tunneling ionization channels. When the electric field is strong, the Keldysh parameter $\gamma = \omega_0\sqrt{m^*\mathcal{E}_g}/(eE_0)$ becomes smaller than 1, where m^* is the effective mass and $\mathcal{E}_g$ is the band gap energy, suggesting the tunneling effects dominate. With our choice of parameters, $\gamma = 1$ corresponds to $E_0 \approx 1.2$ V nm^{-1}. Since tunneling ($\gamma < 1$) occurs much more rapidly than multiphoton absorption [68, 69], the heat bath cannot follow the ionization process and thus has negligible influence at large E_0. In addition, while optical field ionization scales exponentially with E_0, dephasing ionization scales proportional to the laser intensity [14]. As a result, the relative importance of dephasing ionization drops for increasing laser fields. The multi-photon ionization ($\gamma > 1$) develops over an optical cycle and thus is more sensitive to the non-Markovian heat bath, making it more sensitive to heat bath influences.

In order to relate the relative ionization changes to absolute values, ionization in the absence of the heat bath $n_c(j_o = 0, t = \infty)$, is shown as a function of E_0 in figure 5(c). At the highest field strength, ionization is approaching saturation. Moreover, the ionization ratio calculated via the relaxation time approximation is also presented. Comparing figures 5(b) and (c), one can see that the relaxation time approximation predicts orders of magnitude higher ionization compared to that predicted by our model.

4. Discussion

So far, we have seen that the environment can modify ionization by orders of magnitude in the extreme limits of high T or strong coupling j_o. The environment in intense laser-solid interaction is difficult to control. There are various ways in which the environment can be engineered for more controlled experiments on dephasing and dephasing suppressed ionization.

First, light modes in high-quality micro and nano-cavities can be controlled to vary from sub-poissonian, super-poissonian, poissonian, and squeezed vacuum to thermal distributions; from weak to strong coupling with electrons [70, 71]. As such, they can serve as an artificial, strongly coupled environment in which the modification of strong field processes by ionization can be investigated.

Second, collective electron oscillations can be created in tailor-made experiments. The conduction band can be populated by doping semiconductors, or with a pump pulse in a pump-probe experiment. Ionization changes are probed with a second pulse or with transient absorption spectroscopy. As some of the effects observed here depend on strong coupling with the environment, control of the coupling strength is important. Coupling strength increases when going from bulk to 2D and 3D nano-scale materials, such as in nano-resonators and -cavities [72, 73].

Besides, in contrast to a simple two-level system, our two-band model incorporates electron momentum across the entire Brillouin zone. The theoretical framework we develop is general and can be extended to systems with any number of energy bands. To move beyond the basic two-band spin-boson model and address multi-band systems, one can refer to studies [74–76].

The possibility of engineering ionization has potential practical impacts. First, dephasing ionization increases ionization

and thus, allows material micro-machining and -modification at lower laser intensities. This could be instrumental in generating highly charged ion states in high-density plasmas with lower pump pulse energy, contributing to the improvement of table-top x-ray sources. Second, the transition between perturbative nonlinear optics and strong field physics is marked by the onset of ionization. Dephasing suppressed ionization shifts this onset and permits probing dynamics in materials under excitation conditions previously unattainable.

5. Conclusion

The relaxation time approximation is frequently used in intense laser field physics to account for the many-body coupling between a single electron and its environment, which consists of lattice, impurities, and remaining electrons. This work aimed to understand the failure of the relaxation time approximation and to correctly describe ionization in an open quantum system. Ionization in the presence of the relaxation time approximation is enhanced by orders of magnitude over a wide range of parameters, which is termed dephasing ionization.

To decide whether dephasing ionization holds physical significance or is simply a failure of the relaxation time approximation, we have developed a more comprehensive model that captures more physics and still retains much of the simplicity of the relaxation time approximation.

Our results confirmed that ionization enhancement through dephasing ionization still persists, but only in fairly extreme parameter ranges. Very little enhancement is found for acoustical phonon frequencies. For optical phonons and collective electronic excitations dephasing ionization becomes dominant in the limit of high temperatures. Our analysis has also revealed the possibility that a heat bath can suppress ionization by orders of magnitude, which we have named dephasing-suppressed ionization.

We presented a novel framework here to model intense laser many-body processes in a low-cost, semi-phenomenological way. Future research will entail finding realistic environment descriptions beyond the heat bath. Though the SFSB presents a good approximation to a large class of collective excitations of electrons and lattice, it does not account for electron-electron scattering which requires an extended approach with a fermionic heat bath [77]. In particular, the scattering can be included via the Keldysh formalism [78]. Besides, time-dependent heat bath parameters, such as material temperature, are another aspect to be included during intense laser interactions. As such, the ionization dynamics investigated here present only approximate snapshots. For a full treatment of laser material interaction, a dynamically evolving heat bath will have to be considered.

Data availability statement

The data that support the findings of this study are available upon reasonable request from the authors. https://github.com/LuWangPhysics/Heat_Bath_Public.git.

Acknowledgments

T B thanks NSERC for the support. L W thanks Fluffy B for being the motivation to complete this project.

References

[1] Krausz F and Ivanov M 2009 *Rev. Mod. Phys.* **81** 163–234
[2] Goulielmakis E and Brabec T 2022 *Nat. Photon.* **16** 411–21
[3] Haug H and Koch S W 2009 *Quantum Theory of the Optical and Electronic Properties of Semiconductors* (World Scientific)
[4] May V and Kühn O 2023 *Charge and Energy Transfer Dynamics in Molecular Systems* (Wiley)
[5] Jing J, Yu T, Lam C H, You J and Wu L A 2018 *Phys. Rev. A* **97** 012104
[6] Vampa G, McDonald C, Orlando G, Klug D, Corkum P and Brabec T 2014 *Phys. Rev. Lett.* **113** 073901
[7] Du T Y and Ma C 2022 *Phys. Rev. A* **105** 053125
[8] Witzel W M, Carroll M S, Morello A, Cywiński Ł and Das Sarma S 2010 *Phys. Rev. Lett.* **105** 187602
[9] Paz J P, Habib S and Zurek W H 1993 *Phys. Rev. D* **47** 488
[10] Yu T and Eberly J 2003 *Phys. Rev. B* **68** 165322
[11] Ladd T, Maryenko D, Yamamoto Y, Abe E and Itoh K 2005 *Phys. Rev. B* **71** 014401
[12] Kruchinin S Y 2019 *Phys. Rev. A* **100** 043839
[13] Brown G G, Jiménez-Galán A, Silva R E and Ivanov M 2024 *Phys. Rev. Res.* **6** 043005
[14] McDonald C, Taher A B and Brabec T 2017 *J. Opt.* **19** 114005
[15] Nakayama T 1983 *Surf. Sci.* **133** 101–13
[16] Stuart B C, Feit M D, Herman S, Rubenchik A, Shore B and Perry M 1996 *Phys. Rev. B* **53** 1749
[17] Özgür U, Alivov Y I, Liu C, Teke A, Reshchikov M A, Doğan S, Avrutin V, Cho S J and Morkoç H 2005 *J. Appl. Phys.* **98** 041301
[18] Hanif M, Salik M and Baig M 2013 *Plasma Chem. Plasma Process.* **33** 1167–78
[19] Cai X 2020 *Sci. Rep.* **10** 88
[20] Kilen I, Kolesik M, Hader J, Moloney J V, Huttner U, Hagen M K and Koch S W 2020 *Phys. Rev. Lett.* **125** 083901
[21] Brown G G, Jiménez-Galán A, Silva R E and Ivanov M 2024 *J. Opt. Soc. Am. B* **41** B40–B46
[22] Gattass R R and Mazur E 2008 *Nat. Photon.* **2** 219–25
[23] Yanik M F, Cinar H, Cinar H N, Chisholm A D, Jin Y and Ben-Yakar A 2004 *Nature* **432** 822–822
[24] Farsari M and Chichkov B N 2009 *Nat. Photon.* **3** 450–2
[25] Schiffrin A *et al* 2013 *Nature* **493** 70–74
[26] Boolakee T, Heide C, Garzón-Ramírez A, Weber H B, Franco I and Hommelhoff P 2022 *Nature* **605** 251–5
[27] Chlouba T, Shiloh R, Kraus S, Brückner L, Litzel J and Hommelhoff P 2023 *Nature* **622** 476–80
[28] Korolev V *et al* 2024 arXiv:2401.12929
[29] Segal D and Nitzan A 2005 *Phys. Rev. Lett.* **94** 034301
[30] Leggett A J, Chakravarty S, Dorsey A T, Fisher M P, Garg A and Zwerger W 1987 *Rev. Mod. Phys.* **59** 1
[31] Thorwart M, Paladino E and Grifoni M 2004 *Chem. Phys.* **296** 333–44
[32] Lee C K, Moix J and Cao J 2012 *J. Chem. Phys.* **136** 204120
[33] Lambert N, Ahmed S, Cirio M and Nori F 2019 *Nat. Commun.* **10** 3721
[34] Liu Z D, Lyyra H, Sun Y N, Liu B H, Li C F, Guo G C, Maniscalco S and Piilo J 2018 *Nat. Commun.* **9** 3453
[35] Caruso F and Giustino F 2016 *Phys. Rev. B* **94** 115208

[36] Li Z, Antonius G, Wu M, Da Jornada F H and Louie S G 2019 *Phys. Rev. Lett.* **122** 186402
[37] Wang L, Ciappina M F, Brabec T and Liu X 2024 *Phys. Rev. Lett.* **133** 113804
[38] Mahan G D 2013 *Many-Particle Physics* (Springer)
[39] Würger A 1998 *Phys. Rev. B* **57** 347
[40] Nicolin L and Segal D 2011 *J. Chem. Phys.* **135** 164106
[41] Morreau A and Muljarov E 2019 *Phys. Rev. B* **100** 115309
[42] Bundgaard-Nielsen M, Mørk J and Denning E V 2021 *Phys. Rev. B* **103** 235309
[43] Liu H, Zhu L, Bai S and Shi Q 2014 *J. Chem. Phys.* **140** 134106
[44] Thorpe A, Boroumand N, Parks A, Goulielmakis E and Brabec T 2023 *Phys. Rev. B* **107** 075135
[45] Meier C and Tannor D J 1999 *J. Chem. Phys.* **111** 3365–76
[46] Rouse D M, Gauger E M and Lovett B W 2022 *Phys. Rev. B* **105** 014302
[47] Tóth A, Borbély S, Zhou Y and Csehi A 2023 *Phys. Rev. A* **107** 053101
[48] Sussman B J 2011 *Am. J. Phys.* **79** 477–84
[49] Manzano D 2020 *AIP Adv.* **10** 025106
[50] Chen J, Tzou D and Beraun J 2006 *Int. J. Heat Mass Transfer* **49** 307–16
[51] Mozafarifard M, Liao Y, Nian Q and Wang Y 2023 *Int. J. Heat Mass Transfer* **202** 123759
[52] Carpene E 2006 *Phys. Rev. B* **74** 024301
[53] Yamamoto T, Tokura Y and Kato T 2022 *Phys. Rev. B* **106** 205419
[54] Anto-Sztrikacs N and Segal D 2021 *New J. Phys.* **23** 063036
[55] Franchini C, Reticcioli M, Setvin M and Diebold U 2021 *Nat. Rev. Mater.* **6** 560–86
[56] Magazzù L, Forn-Díaz P, Belyansky R, Orgiazzi J L, Yurtalan M, Otto M R, Lupascu A, Wilson C and Grifoni M 2018 *Nat. Commun.* **9** 1403
[57] Devreese J T and Alexandrov A S 2009 *Rep. Prog. Phys.* **72** 066501
[58] Chen C *et al* 2024 *Nature* **636** 342–7
[59] Lugovskoi A, Katsnelson M and Rudenko A 2019 *Phys. Rev. Lett.* **123** 176401
[60] Wu Y, Yu X, Hasaien J, Hong F, Shan P, Tian Z, Zhai Y, Hu J, Cheng J and Zhao J 2024 *Nat. Commun.* **15** 9683
[61] Errea I *et al* 2020 *Nature* **578** 66–69
[62] Goano M, Bertazzi F, Penna M and Bellotti E 2007 *J. Appl. Phys.* **102** 083709
[63] Vampa G, McDonald C, Orlando G, Corkum P and Brabec T 2015 *Phys. Rev. B* **91** 064302
[64] Vampa G, Hammond T, Thiré N, Schmidt B, Légaré F, McDonald C, Brabec T, Klug D and Corkum P 2015 *Phys. Rev. Lett.* **115** 193603
[65] Dufft D, Rosenfeld A, Das S, Grunwald R and Bonse J 2009 *J. Appl. Phys.* **105** 034908
[66] Mishchenko A, Prokof'Ev N, Sakamoto A and Svistunov B 2000 *Phys. Rev. B* **62** 6317
[67] Hofer P P, Perarnau-Llobet M, Miranda L D M, Haack G, Silva R, Brask J B and Brunner N 2017 *New J. Phys.* **19** 123037
[68] Landsman A S, Weger M, Maurer J, Boge R, Ludwig A, Heuser S, Cirelli C, Gallmann L and Keller U 2014 *Optica* **1** 343–9
[69] Klaiber M, Hatsagortsyan K Z and Keitel C H 2015 *Phys. Rev. Lett.* **114** 083001
[70] Wei Y, Liao Z and Wang X H 2024 *Phys. Lett. A* **526** 129965
[71] Najer D *et al* 2019 *Nature* **575** 622–7
[72] Di Giulio V, Akerboom E, Polman A and García de Abajo F J 2024 *ACS Nano* **18** 14255–75
[73] Akerboom E, Di Giulio V, Schilder N J, Garciía de Abajo F J and Polman A 2024 *ACS Nano* **18** 13560–7
[74] Chruściński D, Hesabi S and Lonigro D 2023 *Sci. Rep.* **13** 1518
[75] Merkli M, Berman G and Sayre R 2013 *J. Math. Chem.* **51** 890–913
[76] Reppert M, Reppert D, Pachon L A and Brumer P 2020 *Phys. Rev. A* **102** 012211
[77] Michishita Y and Peters R 2020 *Phys. Rev. Lett.* **124** 196401
[78] Keldysh L V 2024 Diagram technique for nonequilibrium processes *Selected Papers of Leonid V Keldysh* (World Scientific) pp 47–55